J|A|C|S
ARTICLES
Published on Web 05/17/2002

Predictive Concept for Lone-Pair Distortions − DFT and Vibronic Model Studies of $AX_n^{-(n-3)}$ Molecules and Complexes ($A = N^{III}$ to Bi^{III}; $X = F^{-I}$ to I^{-I}; $n = 3-6$)

Michael Atanasov[†,‡] and Dirk Reinen*[,†]

Contribution from Fachbereich Chemie and Zentrum für Materialwissenschaften der Philipps-Universität, Hans-Meerweinstrasse 1, D-35043 Marburg, Germany, and Institute of General and Inorganic Chemistry, Bulgarian Academy of Sciences, Bl.11, Sofia-1113, Bulgaria

Received October 22, 2001. Revised Manuscript Received January 25, 2002

Abstract: The stereochemical and energetic consequences of the lone-pair effect in the title molecules and complexes have been studied by DFT calculations based on a vibronic coupling concept. The anionic complexes were examined as bare entities and, more realistically, in a polarizable charge-compensating solvent continuum. The tendency for distortions of AX_3 compounds away from the high-symmetry parent geometry becomes more pronounced the larger the chemical hardness of a molecule and its constituents is; on the other hand, anionic complexes $AX_n^{-(n-3)}$ ($n = 4-6$) become softer and less susceptible to distortion as compared to the corresponding AX_3 molecule, the larger the coordination number and the anionic charge are. Thus, while all AX_3 compounds adopt the distorted C_{3v} structure, only very few AX_6^{3-} species are calculated to deviate from the parent O_h geometry. If a complex possesses a low stabilization energy due to an unfavorable central ion/ligand size ratio, vibronic coupling may even lead to complete dissociation of one ($SbF_6^{3-} \rightarrow SbF_5^{2-} + F^-$) or more ($PF_6^{3-} \rightarrow PF_4^- + 2F^-$) ligands. The derived *hardness rule* perfectly covers the reported structural findings. The calculations indicate that the lone-pair effect is an orbital overlap phenomenon. The interpair repulsion within the valence shell, keeping the average bond distances constant, does not stabilize the distorted with respect to the parent geometry, in disagreement with the VSEPR model.

I. Introduction

The lone-pair effect is a fascinating phenomenon in the stereochemistry of inorganic compounds and complexes. Though the valence shell electron pair repulsion (VSEPR) model developed by various contributors[1] allows useful predictions concerning the symmetry and approximate geometry of the induced polyhedron distortions, the concept is neither able to specify − starting from the higher symmetry parent geometry observed for the analogous molecules or complexes without the lone pair − the nuclear displacement path leading to the distorted geometry nor able to predict whether a steric effect occurs or not. Reported structural data show that lone-pair compounds may not only frequently possess the undistorted parent geometry, but that they sometimes adopt both the regular and the distorted geometry depending on the particular crystal lattice or even solvent. The physical basis underlying the VSEPR concept has been analyzed by valence bond calculations considering promotion, hybridization, and exchange repulsion.[2] From these and further model studies,[3] it is deduced that interpair repulsion might not be the driving force for a distortion. Furthermore, SCF results suggest that exchange (Pauli) repulsion forces cannot bend the H_2O molecule, for example, without considering classical Coulomb repulsion and orbital overlap energy changes.[4] A more general approach to the nature of the lone-pair effect is the analysis of the vibronic interactions between the nuclear and electronic motions during the distortion process; it has been successfully applied (see Bersuker[5]) in the special form of the second-order or pseudo-Jahn−Teller (PJT) vibronic concept.[6] Here we explicitly mention the recent model studies of Schwerdtfeger[7] and Grochala and Hoffmann, where a correlation of the vibronic coupling strength with the electronegativities of various polyatomic molecules is proposed.[8] Though more

---

* To whom correspondence should be addressed. E-mail: reinen@chemie.uni-marburg.de.

[†] Fachbereich Chemie.

[‡] Bulgarian Academy of Sciences.

(1) Sidgwick, N. V.; Powell, H. M. *Proc. R. Soc.* **1940**, *A176*, 153. Gillespie, R. J.; Nyholm, R. S. *Q. Rev. (London)* **1957**, *11*, 339−380.

(2) Wilson, W.; Doolittle, J.; Edmiston, C. *J. Chem. Phys.* **1973**, *59*, 3020. Ahlrichs, R. *Chem. Unserer Zeit* **1980**, *14*, 18.

(3) Hall, M. B. *J. Am. Chem. Soc.* **1978**, *100*, 6333. Hall, M. B. *Inorg. Chem.* **1978**, *17*, 2261.

(4) Edmiston, C.; Bartleson, J.; Jarvie, J. *J. Am. Chem. Soc.* **1986**, *108*, 3593. Edmiston, C.; Jarvie, J.; Bartleson, J. *J. Chem. Phys.* **1986**, *84*, 6907.

(5) Bersuker, I. B. *The Jahn−Teller Effect and Vibronic Interactions in Modern Chemistry*; Plenum Press: New York, 1984. Bersuker, I. B. *Chem. Rev.* **2001**, *101*, 1067. Bersuker, I. B. *Electronic Structure and Properties of Transition Metal Compounds*; John Wiley and Sons: New York, 1996; Chapter 9: Stereochemistry and Crystal Chemistry and references cited within.

(6) Longuet-Higgins, H. C. *Proc. R. Soc. London, Ser. A* **1956**, *235*, 537. Öpik, U.; Pryce, M. H. L. *Proc. R. Soc. London, Ser. A* **1957**, *238*, 425.

(7) Schwerdtfeger, P.; Hunt, P. In *Advances in Molecular Structure Research*; Hargittai, M., Hargittai, I., Eds.; JAI Press: Stamford, Connecticut, 1999; Vol. 5, p 223.

(8) Grochala, W.; Hoffmann, R. In *Vibronic Interactions: Jahn−Teller Effect in Crystals and Molecules*; Kaplan, M. D., Zimmerman, G. O., Eds; Proceedings of the NATO Advanced Research Workshop on Colossal Magnetoresistance and Vibronic Interactions and the Xvth International Jahn−Teller Symposium, Boston, Aug. 16−22, 2000; Kluwer Academic Publishers: Dordrecht, 2001; p 31. Grochala, W.; Hoffmann, R. *J. Phys. Chem. A* **2000**, *104*, 9740.

10.1021/ja012408h CCC: $22.00

complex than the broadly applicable Gillespie−Nyholm model and its recent extension (ligand close packing),[9] the vibronic coupling model is able to develop rules specifying on which parameters the energy stabilization and the extent of the geometric distortion of a lone-pair polyhedron depend. These parameters can be linked to properties of interest for the chemist, such as the position of the constituents of the considered molecule or complex in the periodic table, the coordination number, etc. However, such a vibronic coupling model becomes very efficient only in combination with quantum-mechanical calculations on the basis of density functional theory (DFT), for example, providing reliable energy and geometric data for a large number of molecules and complexes in a rather short time. We note here that our vibronic analysis refers to the *energy minimum, which characterizes the distorted species*, and not to only small displacements away from the parent geometries, as is usually the case in PJT-type treatments[5] (Supporting Material A).

In a preceding model study[10] we have investigated molecules AH_3 and AX_3 (A = N, P, As, Sb, Bi; X = F, Cl, Br, I) with the interesting finding that the hardness of these entities is the most significant property in predicting lone-pair distortion effects. In the following − after having introduced DFT and the used vibronic interaction model in simple terms in sections II and III − we first give a short review of the previously obtained results[10] for the above-mentioned molecules, with novel extensions and emphasizing the chemical aspects of the lone-pair phenomenon. In the following three sections V−VII, complexes $AX_n^{-(n-3)}$ with coordination numbers (CN) $n = 4-6$ are treated. Here we base our main conclusions − for the sake of a more realistic comparison with experimental data − on the charge-compensated anions in a polarizable solvent continuum (section II).

In a widely used chemical textbook,[11] it is stated that the lone pair becomes less decisive in modifying the stereochemistry of the complex halides of the trivalent elements in the fifth main group, the larger the atomic weight of the central atom and the halogen is, and the higher the coordination number becomes − this remark referring to available structural data. They add that no general and quantitative theory accounting for and predicting such a trend is so far available. Indeed, despite pioneering work by Bader,[12] Bartell,[13,14] and Pearson,[15] who emphasized the importance of bonding effects (the interplay between bonding and nonbonding interactions) for the stereochemical activity of lone pairs within the frame of a PJT formalism, and later model studies,[16] this statement is still valid. It is the ambitious aim of this contribution to present a sensible model accomplishing this, based on DFT calculations. We are not aiming at high numerical accuracy, but present an empirical vibronic model adjusted to DFT energies and geometries, with the emphasis laid on the chemical and structural relevance.

II. Computational Details

The calculations were carried out using the Amsterdam density functional (ADF) program version 2000.02 developed by Baerends et al.[17] Calculated total energies and geometry optimizations are based on the gradient corrected exchange functional of Becke[18] and the correlation functional of Perdew[19] in conjunction with the LDA parametrization of Vosko et al.[20] Molecular orbitals and electronic configurations of $AX_n^{(n-3)-}$ complexes are approximated by a triple-ζ basis set for both A and X, including scalar relativistic corrections for all studied clusters. Utilizing the extended transition state method by Ziegler and Rauck,[21] the total energy E_t is decomposed into three terms. The most significant of these in the context of the Gillespie−Nyholm model is the overlap between the closed shells of the unrelaxed fragments of the considered molecules or complexes, giving rise to the Pauli exchange repulsion term (E_P). The electrostatic energy (E_{el}) accounts for the Coulomb repulsion between the nuclei and between the electrons of different fragments and for the Coulomb attraction between electrons on one fragment and nuclei of all the other unrelaxed fragments. The relaxation of the electron density by the charge transfer when exciting electrons from doubly and singly occupied fragment orbitals into empty or singly occupied MOs is allowed for by the orbital interaction energy E_{orb}. We focus our main interest on the changes of these quantities during the transition from the high-symmetry parent to the distorted geometry: δE_P, δE_{el}, and δE_{orb}. These crucially depend on the reference, if the chosen fragments are atoms or ions, for example. Only the change of the total energy δE_t is independent of the fragment choice. Thus, starting from atomic fragments, δE_{orb} will not only reflect attractive interactions due to overlap between atomic orbitals (covalency), but also repulsive $X^- \leftrightarrow X^-$ interactions induced by the A $\leftrightarrow$ X charge transfer. In the case of ionic fragments, δE_{orb} is usually rather different, depending on the effective charges of the fragments of the considered molecule or complex. We interpret[10] δE_P as representing mainly the steric repulsion energy, which is considered to govern the change from the parent to the distorted geometry by the VSEPR model, the latter implying that the repulsion within the set of bonding electron pairs and the lone pair in a molecule or complex is more favorable in the distorted than in the high-symmetry parent geometry. Though δE_P is defined for the unrelaxed fragments, and hence orbital contributions stemming from (antibonding) interactions between doubly occupied MOs are expected to add to the steric repulsion energy by the relaxation process, this correction will be small. In the following, we base our analysis on atomic fragments as the reference, which is a more realistic choice for isolated molecules or complexes than the one of ionic fragments pertinent to ionic solids.

Highly charged anions are known to be intrinsically unstable against dissociation into less charged species. However, stabilization by the Madelung potential created by counterions in solids may change the situation thoroughly. To (in the average) mimic such electrostatic stabilization of charged species, while keeping the treatment as general as possible, we used an isotropic polarizable dielectric continuum within the so-called conductor-like screening model (COSMO) of solvation.[22]

---

[9] Gillespie, R. J.; Robinson, E. A. *Angew. Chem.* **1996**, *108*, 539 [*Int. Ed. Engl.* 495]. Gillespie, R. J. *Coord. Chem. Rev.* **2000**, *197*, 51.

[10] Atanasov, M. A.; Reinen D. *J. Phys. Chem. A* **2001**, *105*, 5450.

[11] Greenwood, N. N.; Earnshaw, A. *Chemistry of the Elements*, 2nd ed.; Butterworth & Heinemann: Oxford, 1998.

[12] Bader, R. F. W. *Mol. Phys.* **1960**, *3*, 137.

[13] Bartell, L. S. *J. Chem. Educ.* **1968**, *45*, 754.

[14] Bartell, L. S. *Coord. Chem. Rev.* **2000**, *197*, 37.

[15] Pearson, R. G. *J. Am. Chem. Soc.* **1969**, *91*, 4947−4955. See also Pearson, R. G. *Symmetry Rules for Chemical Reactions, Orbital Topology, and Elementary Processes*; John Wiley and Sons: New York, 1976.

[16] Dolg, M.; Küchle, W; Stoll, H.; Preuss, H.; Schwerdtfeger, P. *Mol. Phys.* **1991**, *74*, 1265. Klobukowski, M. *Can. J. Chem.* **1993**, *71*, 141. Klobukowski, M. *J. Comput. Chem.* **1993**, *14*, 1234. Crawford, T. D.; Springer, K. W.; Schaefer, H. F., III. *J. Chem. Phys.* **1995**, *102*, 3307. Marian, C. M.; Peric, M. Z. *Z. Phys. D: At., Mol. Clusters* **1996**, *36*, 285. Kaup, M; van Wüllen, Ch.; Franke, R.; Schmitz, F.; Kutzelnigg, W. *J. Am. Chem. Soc.* **1996**, *118*, 11939.

[17] Baerends, E. J.; Ellis, D. E.; Ros, P. *Chem. Phys.* **1973**, *2*, 41−51. Baerends, E. J.; Ros, P. *Int. J. Quantum Chem. Symp.* **1978**, *12*, 169. Baerends, E. J.; Ros, P. *Chem. Phys.* **1973**, *2*, 52. Boerrigter, P. M.; te Velde, G.; Baerends, E. J. *Int. J. Quantum Chem.* **1988**, *33*, 87. te Velde, G.; Baerends, E. J. *J. Comput. Phys.* **1992**, *99*, 84 and references therein. For an excellent review of the present status of ADF see: te Velde, G.; Bickelhaupt, F. M.; Baerends, E. J.; Fonesca Guerra, C.; van Gisbergen, S. J. A.; Snijders, J. G.; Ziegler, *J. Comput. Chem.* **2001**, *22*, 931.

[18] Becke, A. D. *Phys. Rev. A* **1988**, *38*, 3098−3100.

[19] Perdew, J. P. *Phys. Rev. B* **1986**, *33*, 8822−8824.

[20] Vosko, S. H.; Wilk, L.; Nusair, M. *Can. J. Phys.* **1980**, *58*, 1200.

[21] Ziegler, T.; Rauk, A. *Theor. Chim. Acta* **1977**, *46*, 1. Ziegler, T.; Rauk, A. *Inorg. Chem.* **1979**, *18*, 1558, 1755. Diefenbach, A.; Bickelhaupt, F.; Matthias; Frenking, G. *J. Am. Chem. Soc.* **2000**, *122*, 6449.

It is implemented in the ADF2000.02 program,[23] and not only allows single point calculations, but geometry optimizations and Hessian computations as well. We chose the dielectric constant of water ($\epsilon = 78.4$) and a solvent-excluding surface around the solute, with the solvent molecule, approximated as spherical ($R_{\mathrm{solv}} = 1.4$ Å for water), rolling around the van der Waals surface (VdW) of the "dissolved" species. Atomic radii for solvent calculations are still scarce, and we mainly restrict to $\mathrm{PF}_n{}^{-(n-3)}$ clusters with $R_{\mathrm{P}} = 2.4$ Å[23] and $R_{\mathrm{F}} = 1.4$ Å,[24] as compared to the analogous $\mathrm{Al^{III}}$ polyhedra ($R_{\mathrm{Al}} = 2.3$ Å[25]), but also included $\mathrm{B^{III}}$ ($R_{\mathrm{B}} = 1.2$ Å[26]) in comparison to $\mathrm{N^{III}}$ ($R_{\mathrm{N}} = 1.6$ Å[24]). In the case of $\mathrm{SbF}_n{}^{-(n-3)}$, the unknown radius of $\mathrm{Sb^{III}}$ (R_{Sb}) has been estimated using the relation $R_{\mathrm{Sb}}/R_{\mathrm{Sb}}(\mathrm{VdW}) = R_{\mathrm{P}}/R_{\mathrm{P}}(\mathrm{VdW})$ with $R_{\mathrm{Sb}}(\mathrm{VdW}) = 2.0$,[27] $R_{\mathrm{P}}(\mathrm{VdW}) = 1.8$[20], and $R_{\mathrm{P}} = 2.4$ Å, yielding $R_{\mathrm{Sb}} = 2.7$ Å.

In the presence of a solvent, the solute−solvent interaction or solvation energy (E_{solv}) comes additionally into play. The energy changes accompanying the structural transition, without (1a) and with solvent (1b), are accordingly:

$$\delta E_{\mathrm{t}} = \delta E_{\mathrm{P}} + \delta E_{\mathrm{el}} + \delta E_{\mathrm{orb}} \tag{1a}$$

$$\delta E_{\mathrm{t}}{}' = \delta E_{\mathrm{P}}{}' + \delta E_{\mathrm{el}}{}' + \delta E_{\mathrm{orb}}{}' + \delta E_{\mathrm{solv}} \tag{1b}$$

While δE_{P}, δE_{el}, and δE_{orb} may change considerably, when placing the considered species into the solvent medium ($\rightarrow \delta E_{\mathrm{P}}{}'$, $\delta E_{\mathrm{el}}{}'$, $\delta E_{\mathrm{orb}}{}'$), the sum is nearly constant ($\delta E_{\mathrm{t}}{}' - \delta E_{\mathrm{solv}} \cong \delta E_{\mathrm{t}}$). Also, δE_{solv} is small, though ($-E_{\mathrm{solv}}$) increases considerably with increasing charge. When choosing a solvent with ϵ about one-half that of $\mathrm{H_2O}$, such as acetonitrile ($\epsilon = 36.6$, $R_{\mathrm{ac}} = 2.06$ Å;[28] in parentheses), no dramatic change is observed:

	$\mathrm{PF_4{}^-}$	$\mathrm{PF_3}$	$\mathrm{F^-}$	
$E_{\mathrm{t}}{}'$	−28.44(−28.62)	−19.54(−19.54)	−8.45(−8.38)	eV
E_{solv}	−2.60(−2.48)	−0.05(0.0.05)	−4.46(−4.39)	eV

DFT orbitals and their energies have been calculated by solving the Kohn−Sham equations, where both electronic exchange and correlation were taken into account. The orbital energies of a specific bare anion shift by about the same amount to higher energies when compared with the charge-compensated complex. Thus the highest occupied orbitals may adopt positive energy values, implying instability with respect to self-ionization, even though the anions are calculated to possess a relative energy minimum. We will hence base our analysis of the MOs and the underlying bonding effects mainly on the more realistic solvated species.

The vibrational energies of the bare anions are strongly different from those of the charge-compensated species, precluding a direct comparison with experiment. Taking octahedral $\mathrm{PF_6{}^{3-}}$ as an example, the α_{1g} and ϵ_{g} modes shift to much higher energies when proceeding to the solvated anion (336 → 414 and 168 → 241 $\mathrm{cm^{-1}}$, respectively). The τ_{2g}, the τ_{2u}, and the lower-energy τ_{1u} modes are less affected (179 → 171, 126 → 128, −149 → −164 $\mathrm{cm^{-1}}$), the negative numbers denoting an imaginary frequency and hence configurational instability. Similarly, calculated vibrational energies of the bare $\mathrm{SbBr_6{}^{3-}}$ anion [114 (α_{1g}), 83 (ϵ_{g}), 52 (τ_{2g}), 44,122 ($2x\tau_{1u}$), and 34 (τ_{2u}) $\mathrm{cm^{-1}}$] are strongly underestimated if compared with the experimental values [180 (α_{1g}), 153 (ϵ_{g}), 73 (τ_{2g}), 107,180 ($2x\tau_{1u}$) $\mathrm{cm^{-1}}$]. From our calculations on $\mathrm{PF_6{}^{3-}}$, a solvent can account only to a limited extent for such influences, because kinematic effects due to the finite masses of the surrounding solvent are completely ignored. Therefore, we use the vibrational energies only as a semiquantitative tool for the exploration of certain trends governing the lone-pair activity.

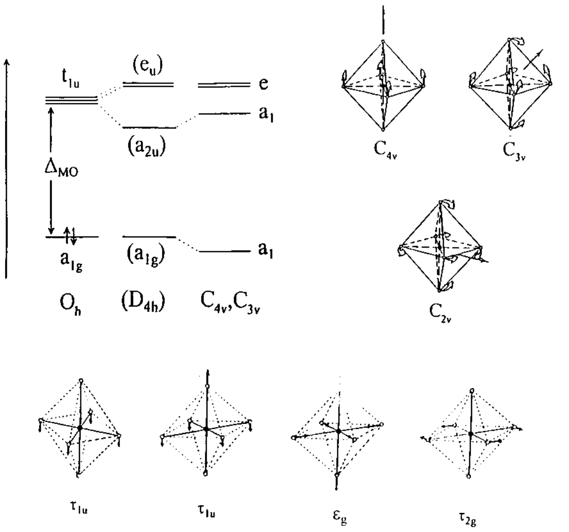

Figure 1. The HOMO (from ns) and LUMO (from np) − initial splitting Δ_{MO} − in the MO scheme for an octahedral lone-pair $\mathrm{A^{III}}$ complex and their vibronic interaction, resulting in C_{4v}, C_{3v}, and C_{2v} (here e splits in $\mathrm{b_1}$ and $\mathrm{b_2}$ additionally) distortion geometries: $\mathrm{a_{1g}} \otimes \tau_{1u} \otimes \mathrm{t_{1u}}$; the first-order Jahn−Teller splitting of the excited $\mathrm{t_{1u}}$ state is indicated. The four high-symmetric components of the $\tau_{1u}(2x)$, ϵ_{g}, and τ_{2g} octahedral vibrational modes as well as the linear combinations of τ_{1u} according to C_{2v}-, C_{3v}-, and C_{4v}-type displacements are also depicted.

III. The Vibronic Coupling Model

If one looks at coordinated lone-pair cations starting from the highest possible symmetry, say the octahedral O_h for the coordination number CN = 6, and considers nuclear motions along certain normal mode distortion coordinates, these may lead into lower-symmetry point groups with decreased energy. The critical condition for the selected modes v with such a property is that the HOMO − here of $\mathrm{a_{1g}}$ symmetry, which houses the lone pair (mostly $\mathrm{ns^2}$) − and the LUMO or a split state of the LUMO (in O_h: $\mathrm{t_{1u}}$, originating from the metal np orbitals) adopt the same symmetry, thus inducing an interaction, which stabilizes the HOMO (Figure 1). Group theory allows one to select the possible vibronically active vibrations v by inspecting the direct product, $\mathrm{a_{1g}} \otimes v \otimes \mathrm{t_{1u}}$ in O_h, which has to contain the totally symmetric representation (second-order or pseudo-Jahn−Teller effect, PJTE[6]). This is in $\mathrm{ns^2}$ lone-pair systems always the case, if the vibrational modes possess the same symmetry as the LUMO. In octahedral coordination, the stretching and bending τ_{1u} vibrations (Figure 1) obey this condition. Hence, any linear combination j of the three $\tau_{1u}(i)$ components ($i = z, x, y$) will eventually lead into distorted coordination polyhedra with decreased energy. The highest possible distortion symmetries along these pathways are $j = C_{4v}$ [$\tau_{1u}(z)$], C_{3v} [$(1/\sqrt{3})(\tau_{1u}(z) + \tau_{1u}(y) + \tau_{1u}(x))$], and C_{2v} [$(1/\sqrt{2})(\tau_{1u}(x) + \tau_{1u}(y))$], inducing the (5 + 1), (3 + 3), and (4 + 2) coordinations shown in Figure 1. From the two τ_{1u} modes in O_h, only one exhibits soft mode behavior, with mixed bending and stretching properties (section VII). The corresponding energy matrix contains, via the $N(i)$ term, the distortion coordinates $\tau_{1u}(i)$ and the vibronic coupling constant t, which controls the strength of the $\mathrm{a_{1g}}$−$\mathrm{t_{1u}}$ electronic interaction:

---

(22) Klamt, A.; Schüürmann, G. *J. Chem. Soc., Perkin Trans. 2* **1993**, 799.
(23) Pye, C. C.; Ziegler, T. *Theor. Chim. Acta* **1999**, *101*, 396.
(24) Klamt, A.; Jonas, V. *J. Chem. Phys.* **1996**, *105*, 9972.
(25) Zurek, E.; Ziegler, T. *Inorg. Chem.* **2001**, *40*, 3279.
(26) Vanka, K; Chan, M. S. W.; Pye, C. C.; Ziegler, T. *Organometallics* **2000**, *19*, 1841.
(27) Bondi, A. *J. Phys. Chem.* **1964**, *68*, 441.
(28) *Handbook of Chemistry and Physics*, 76th ed.; Lide, D. R., Ed.; CRC Press: Boca Raton, 1995−1996.

$$\begin{array}{llllll} A_{1g}(s^2) & E_g - E & N(x) & N(y) & N(z) & \\ T_{1u}x(s^1p_x^1) & N(x) & E_e - E & 0 & 0 & \\ T_{1u}y(s^1p_y^1) & N(y) & 0 & E_e - E & 0 & N(i) = t\tau(i) \\ T_{1u}z(s^1p_z^1) & N(z) & 0 & 0 & E_e - E & \end{array} \qquad (2)$$

It uses many electron states (A_{1g}, T_{1u}) rather than just considering the HOMO and LUMO − according to the $A_{1g} \otimes \tau_{1u} \otimes T_{1u}$ direct product − because the vibronic coupling includes all MOs of a_{1g} and t_{1u} symmetry in the respective MO scheme. It is confined to a two-state system, restricting to the ground state and only the lowest among other excited T_{1u} states of higher energy, which can also mix with the ground state. Our calculations show that the *two-state approximation* works rather well in the case of the AX_3 molecules[10] (Appendix).

E_g and E_e are the energies of the interacting ground and excited state, the energy difference being the initial splitting δ. The general equation for the stabilization energy of the ground state resulting from vibronic matrixes of the kind (eq 2) has the form:

$$\begin{aligned} E_-{}^m &= E_g{}^m + (^1/_2)\delta E_{g,e}{}^m - \{(\delta E_{g,e}{}^m/2)^2 + N^{m2}\}^{1/2} \qquad (3) \\ &\equiv E_{rf}{}^m - E_{vib}{}^m \end{aligned}$$

where the upper index m denotes that all energies are those characteristic for the minimum of the potential curves (see Figure 7a) in the distorted geometry. $E_g{}^m$ and $E_e{}^m$ ($\delta E_{g,e}{}^m = E_e{}^m - E_g{}^m$) are the hypothetical energy values of the ground and excited state, respectively, in the case of vanishing nondiagonal coupling terms N, but leaving the nuclear displacements as in the optimized distorted geometry. $E_{vib}{}^m$ is the vibronic energy induced by the distortion process (eq 4) and is composed of a diagonal contribution connected with $\delta E_{g,e}{}^m$ − accounting for the admixture of an $E_e{}^m$ component into the ground-state $E_g{}^m$ energy − and the symmetry-breaking nondiagonal N^m term. $E_{rf}{}^m$ is the energy necessary for the geometric change from the parent to the distorted structure without taking vibronic coupling into account ($N = 0$) and is, as in the considered cases, usually a positive quantity (see ref 4, however).

$$\begin{aligned} E_{vib}{}^m &\equiv (^1/_2)(E_{FC}{}^m - \delta E_{g,e}{}^m) \\ E_{FC}{}^m &= 2\{(\delta E_{g,e}{}^m/2)^2 + (N^m)^2\}^{1/2} \qquad (4) \\ E_{rf}{}^m &\equiv E_g{}^m \end{aligned}$$

The square root (eq 4) corresponds to one-half of the final splitting $E_{FC}{}^m = E_+{}^m - E_-{}^m$, the Franck−Condon energy between the excited and the ground state in the distorted geometry, an observable quantity. Figure 2 illustrates the energetic situation, the numerical data being those of BiF_3 during the D_{3h} to C_{3v} transition (section IV).

We did not include the first-order Jahn−Teller splitting of the excited T_{1u} state into matrix 2, which may occur along the pathways of the ϵ_g (stretching) and τ_{2g} (bending) vibrations in O_h; here, usually the coupling to the ϵ_g mode dominates, leading into the D_{4h} point group (see Figure 1). Because excited-state properties are admixed to the ground state via the nondiagonal PSJT-coupling element N, the complex geometry and stabilization energy are influenced by this effect (section VII). With this in mind, the C_{4v} distortion, which differs from D_{4h} by the missing inversion center, is expected to be favored most.

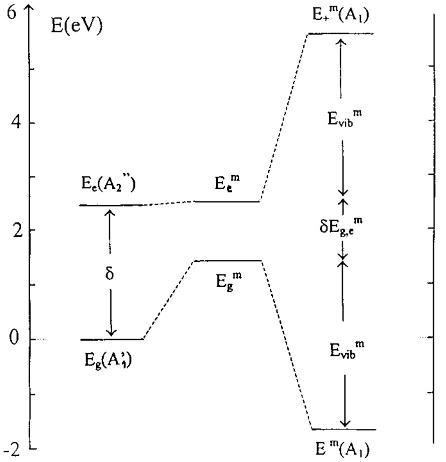

Figure 2. The energy changes of the BiF_3 molecule − $A_1' \otimes \alpha_2'' \otimes A_2''$ PJT-coupling, $D_{3h} \rightarrow C_{3v}$ transition according to the vibronic model (eqs 3, 4).

We show in the next four sections that the vibronic coupling model exactly predicts all possible distortion geometries and develops criteria, whether a distortion occurs or not. We finally remark that we will use the notation *vibronic coupling* exclusively for the lone-pair phenomenon, as connected with the nondiagonal elements of matrix (eq 2) in the following. We thus confine the usually broad definition of vibronic coupling as any process connected with the interaction between nuclear and electronic motions to a specific phenomenon.

IV. The Coordination Number CN = 3

In accord with the experimental data, the three-coordinate compounds AH_3 and AX_3 (A = N to Bi; X = F to I) are calculated by DFT to possess pseudotetrahedral structures AH_3E and AX_3E (E = lone pair), as expected by the VSEPR model of Gillespie−Nyholm.[1,9] The distortions from the hypothetical planar high-symmetry parent geometry D_{3h} toward the trigonal pyramid C_{3v} (Figure 3) are accompanied not only by large angular (bond angle) changes according to the vibronically active symmetry-breaking α_2'' vibration, but also by significant radial alterations (bond length reduction in the case of AX_3E and bond length extension in the case of AH_3E) according to the totally symmetric α_1' stretching mode.[10] Here, it is striking to note that the Pauli interaction energy δE_p, and δE_{el} as well, is only sensitive with respect to the radial changes, while it remains approximately constant during the α_2''-type displacements (Table 1). *The driving force for the steric lone-pair effect is a pure bond energy change* stemming from δE_{orb}, in accord with earlier statements.[5,13] Hence, we conclude from the DFT analysis that *the repulsion between the bonding and lone electron pairs − which should be energetically more favorable in the distorted structure according to the VSEPR concept − does not hold.* δE_P, which can be considered to represent essentially the VSEPR energy (section II), nearly vanishes if solely displacements according to the symmetry-breaking (sb) α_2'' mode are considered ($\delta E_P{}^{sb} \cong 0$). It is challenging to check whether this result holds for the higher coordination numbers as well.

As is readily deduced from the Kohn−Sham MO scheme for PF_3 (Figure 3), the HOMO and LUMO are of $a_1'(3a_1')$ and

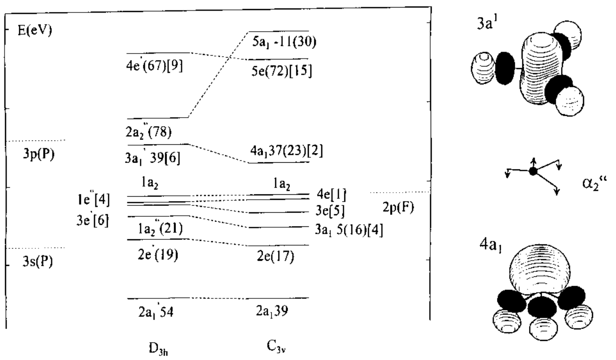

Figure 3. MO scheme of solvated PF_3 for DFT optimized D_{3h} and C_{3v} geometries, with the 3s, 3p (in parentheses) and 3d (in square brackets) P contributions (%) indicated (left). The symmetry-adapted LCAOs in D_{3h} originating from the ligand 2s and 2p orbitals are a_1'; $e'(\sigma)$ and $a_1'(\sigma)$; $2xe'(\sigma,\pi$ in-plane); $a_2''(\pi$ out-of-plane); a_2',e''(nonbonding) − those from metal 6s and 6p are $a_1'(\sigma)$ and $a_2''(\pi$ out-of-plane), $e'(\sigma,\pi$ in-plane); the low-lying $1a_1'$ and $1e'$ MOs at ≅−30.3 eV are nearly nonbonding with respect to the ligand 2s AOs and not shown. The energies of the parent P(3s,3p) and ligand F(2s,2p) AOs for the effective charges of P and F in D_{3h} were estimated making use of the Kohn−Sham orbital energies and eigenfuctions. The wave functions (ψ) underlying the lone-pair HOMO in D_{3h} (above) and C_{3v} (below), and the active α_2'' mode are also shown. The contour plot diagram is constructed for ±0.1 values of ψ; small P(3d) contributions are seen in $3a_1'$.

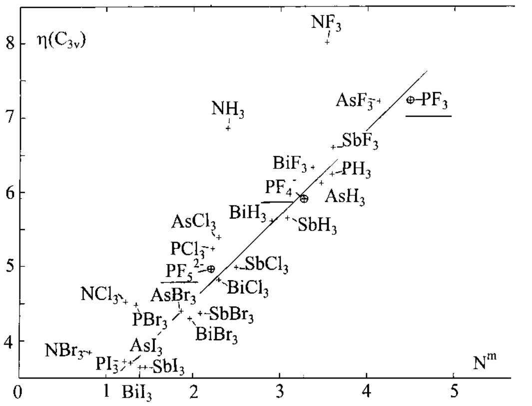

Figure 4. Energy plot (eV) of $\eta(C_{3v})$ versus N^m (eqs 3−6) for AX_3 and AH_3 molecules and the charge-compensated PF_4^- and PF_5^{2-} complexes − here, η (C_{2v}) and η (C_{4v}), respectively (straight line: least-squares fit).

$a_2''(2a_2'')$ symmetry. In the many electron description, $A_1'(ns^2)$ and $A_2''(ns^1p_z^1)$ are the interacting states, implying an $A_1' \otimes \alpha_2'' \otimes A_2''$ direct product. From the a_1' and a_2'' MOs in D_{3h} involved in the vibronic process, particularly the HOMO is strongly stabilized (by −1.4 eV). It is apparently the energy gain of the lone pair occupying this HOMO (−2.8 eV) which contributes most to $\delta E_t \equiv E_-^m$ (−2.7 eV). New bonds are created by $s-p_z$ mixing, which is allowed in C_{3v} but forbidden in D_{3h}. The lone pair adopts directional properties by the vibronic process (Figure 3), sticking out toward the fourth ligand position of a hypothetical tetrahedron (AX_3E). As has been discussed elsewhere,[10] the molecules AH_3 and NX_3 possess $p_z^2(a_2''^2)$-type lone pairs, in contrast to the bulk of the considered compounds with $A_1'(a_1'^2)$ ground and $A_2''(a_1'^1a_2''^1)$ excited states.

The DFT energy $\delta E_{orb}(a_1)$ represents the energy changes of only those MOs which are involved in the vibronic process (Table 1). N^m is − see the preceding section − the quantity which comprises part of this energy, induced by the nondiagonal vibronic coupling. Additional shifts of the a_1 MOs are caused by the mixing of excited-state properties into the ground state and vice versa (diagonal vibronic effect), on one hand, and by the geometric changes during the $D_{3h} \rightarrow C_{3v}$ transition − the latter contributing to E_{rf}^m − on the other hand (eqs 3, 4). N^m is predominantly due to the α_2'' displacements with only a small participation (≤10%) of the α_1'-type bond length alterations.[10] In contrast to the DFT energy changes δE_{orb}, δE_P, δE_{el} − which depend on the chosen reference fragments (section II) − N^m is an invariant. The DFT and the vibronic energy increments correspond to a rather different partition of the total energy change $\delta E_t = E_-^m$, yielding complementary physical insight.

Table 1. Energies from DFT Calculations (eV): Contributions from Symmetry-Breaking Modes Solely, First Line; Total Energies without and with Solvent, Second and Third Line, Respectively

	δE_P	δE_{el}	δE_{orb}	$\delta E_{orb}(a_1)$	$\delta E_t(')$
PF_3	0.18	−0.09	−2.43	−7.39	−2.34
	12.85	−4.16	−11.36	−11.15	−2.67
	13.13	−4.26	−11.60	−11.22	−2.65[a]
SbF_3	0.06	−0.02	−1.51	−4.74	−1.47
	6.59	−2.40	−5.85	−6.62	−1.66
PF_4^-	1.36	−0.38	−2.20	−0.79	−1.23
	17.39	−5.54	−13.55	−5.48	−1.70
	13.74	−4.35	−11.04	−5.81	−1.78[a]
SbF_4^-	0.65	−0.14	−0.99	0.03	−0.48
	7.47	−2.58	−5.54	−1.67	−0.65
PF_5^{2-}	1.13	−0.35	−1.40	−0.81	−0.62
	12.42	−4.00	−9.30	−3.50	−0.88
	14.75	−4.77	−10.74	−4.91	−1.06[a]
SbF_5^{2-}	0.60	−0.17	−0.68	0.08	−0.25
	6.07	−2.10	−4.32	−1.26	−0.36

[a] $\delta E_t'$ (eq 1b): contains the solute−solvent interaction energy δE_s of 0.03, −0.13, and −0.29 eV for PF_3, PF_4^-, and PF_5^{2-}, respectively.

The Franck−Condon energy E_{FC}^m (eq 4) is expected to be correlated with the chemical hardness (eq 6); this is so because I and A increase and decrease, respectively, if the excited A_2'' state wave function is admixed to the A_1' ground-state wave function.[29] In the case of the considered molecules, $(N^m)^2$ is mostly very large with respect to $(\delta E_{g,e}^m/2)^2$ in eq 4, yielding in good approximation eq 5. This implies, as has been substantiated elsewhere,[10] that N^m depends approximately linearly on the chemical hardness η (eq 6).

$$(^1/_2)E_{FC}^{m} \cong N^{m} \qquad (5)$$

Both quantities N^m and $\eta(C_{3v})$ increase in the sequence I → Br → Cl → H → F and, less pronounced, from Bi to P (for the

$$\eta = (I - A)/2$$
$$(I\text{, ionization energy; } A\text{, electron affinity}) \qquad (6)$$

hydrogen and fluoride compounds). *The harder the molecules and their atomic constituents are, the more susceptible to lone-pair distortions they become (Figure 4).* A similar result is reported in a recent investigation on lead(II) compounds, where the stabilization energies on distortion come out to be larger the harder the ligand and the lower the coordination number is.[30] Deviations from the *hardness rule* may occur in the case of large initial splittings δ (NH_3, NF_3) − here condition (eq 5) is not satisfied − and if the two-state approximation does not strictly hold (NX_3 with X = F to I). If N^m is considerably smaller than δ, the vibronic energy is approximately

---

(29) Pearson, R. G. *Chemical Hardness*; Wiley-VCH: Weinheim-New York, 1997; pp 89−95.

(30) Shimoni-Livny, L.; Glusker, J. P.; Bock, C. W. *Inorg. Chem.* **1998**, *37*, 1853.

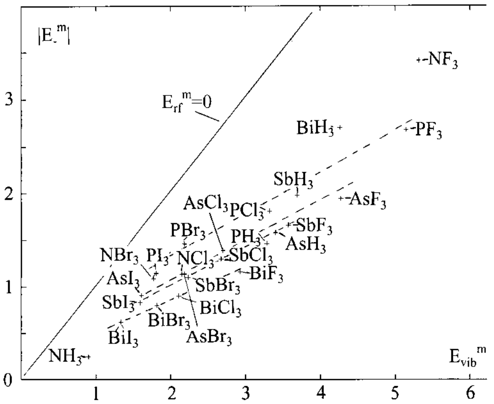

Figure 5. Energy plot (eV) of $|\delta E_t| = |E_-^m|$ versus E_{vib}^m (eqs 3−5) for AX_3 molecules with s^2-type and for AH_3 compounds with p_z^2- ground states in D_{3h}. The deviations from the full line are the restoring energies E_{rf}^m; the hatched lines indicate increasing E_{rf}^m values in the sequence $I^- \rightarrow F^-$.

$$E_{vib}^{\ m} \cong -N^{m2}/\delta \tag{3a}$$

We further show in Figure 5 how the energy stabilization $|\delta E_t| = |E_-^m|$ depends on the vibronic coupling energy $E_{vib}^m \cong N^m - (^1/_2)\delta E_{g,e}^m$ (eqs 4, 5). The deviations from the full line represent the restoring energies, which increase from the iodides to the fluorides (see hatched lines) and, less pronounced, from Bi to P, as expected. It is also striking that the hardest molecules possess the largest vibronic energies E_{vib} and the largest stabilization energies $|E_-^m|$. This is not the case for the molecules with p_z^2- ground states (the hydrides and the NX_3 molecules), which represent a rather exotic type of compounds within the lone-pair families.[10] Nevertheless, Figure 4 presents evidence that the nondiagonal vibronic coupling energy N^m is the energetically determining quantity for the distortion process in the case of s^2-type lone pairs, at least for the three-coordinate molecules considered here. We finally note that the inclusion of a polarizable solvent does not affect the DFT energies significantly (Table 1), as expected for an entity without charge.

V. The Coordination Number 4

Geometric instability of a tetrahedral complex AX_4^- may occur if the a_1 HOMO, housing the ns^2-type lone pair, which is antibonding and strongly delocalized toward the ligands, interacts with the LUMO of t_2 symmetry originating from the 3p(P) AOs (Figure 6). The admixture donates directional properties to the lone pair, thus inducing a distortion, whose symmetry is determined by the two vibronically active τ_2 modes ($A_1 \otimes \tau_2 \otimes T_2$ PJT-coupling) − one of stretching and one of bending nature (Figure 6a). The highest symmetry distortions lead into C_{3v} and C_{2v} point groups, the former being induced by an equal mixture of all three τ_2 components and the latter corresponding to just one component (lone-pair orientation $||C_3$ and $||C_2$, respectively). Both pathways yield pseudotrigonal-bipyramidal AX_4E geometries; in the C_{2v} case, the lone pair is located in the equatorial plane [$A(X_2E)X_2$], while it takes the position of an axial ligand in C_{3v} [$A(X_3)(XE)$]. The vibronic interaction matrix is analogous to that of eq 2. The coupling occurs with the τ_2 mode possessing the lower frequency, which is characterized by both bending and stretching properties. Similar to the octahedral case, the excited 3-fold degenerate state is Jahn−Teller unstable with respect to some active vibrations in T_d [T_2- ($\epsilon + \tau_2$) problem].[5] The excited-state admixture to the ground state via the nondiagonal coupling term N is thus expected to add distortion components along ϵ (see Figure 6a) to the final complex geometry. The latter influence is indeed striking and would lead into the D_{2d} point group; the S_4 axis in the final C_{2v} symmetry is lost, however.

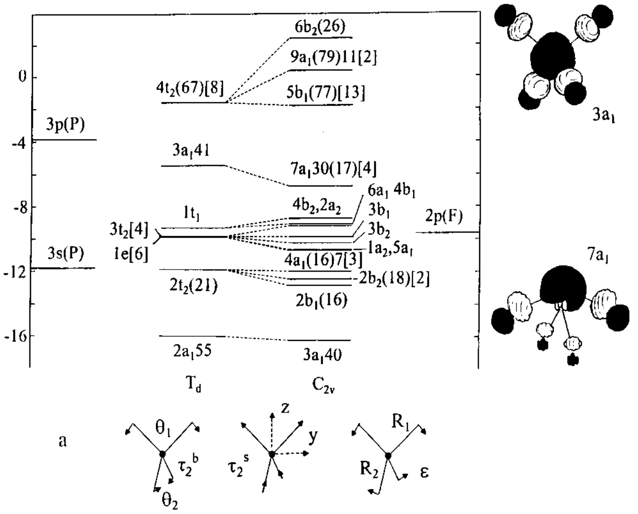

Figure 6. MO scheme of the PF_4^- complex (energies in eV) in a solvent continuum for DFT optimized T_d and C_{2v} geometries, with the 3s, 3p (in parentheses), and 3d (in square brackets) phosphorus contributions (%) indicated. The symmetry-adapted LCAOs in T_d originating from the ligand 2s and 2p AOs are $a_1(\sigma)$; $t_2(\sigma)$ and $a_1(\sigma)$; $t_2(\sigma + \pi)$; e, t_1, t_2 (nonbonding), respectively; the P(3s,3p) AOs transform as $a_1(\sigma)$; $t_2(\sigma + \pi)$. The T_d MOs transform in C_{2v} as follows: $e \rightarrow a_1,a_2$; $t_1 \rightarrow a_2, b_1, b_2$; $t_2 \rightarrow a_1(||z), b_1(||x), b_2(||y)$. The energies of the parent P(3s,3p) and ligand F(2s,2p) AOs for effective charges of P and F in T_d were estimated making use of the Kohn−Sham orbital energies and eigenfuctions. The nonbonding $1a_1$ and $1t_2$ MOs from 2s(F) at ∼−28.5 eV are not shown. The wave functions underlying the lone-pair HOMO in T_d and the resulting MO in C_{2v} are also depicted. (a) The $T_d \rightarrow C_{2v}$ ligand displacements according to the z-component of the bending and stretching τ_2 modes, as well as the higher-symmetry component of the ϵ mode.

Inspecting complexes of the type AX_4^- (A = N to Bi; X = F to I), we find that, in contrast to the AX_3 molecules, only part of them exhibit lower-symmetry distortions. Leaving aside the NX_4^- polyhedra at this stage, the tetrahedra with the highest hardness values are predicted by DFT to distort. This is in agreement with the trends in Figure 4, where such molecules are observed to be the most sensitive to vibronic coupling. Furthermore, it turns out that in these cases the C_{2v} distortion is more stable than the C_{3v} geometry, which is still preferred with respect to T_d, however. As has been explicitly checked, all vibrational frequencies are real in C_{2v}, the corresponding minima thus representing genuine and absolute minima of the ground state. In contrast, the T_d geometry is characterized by one imaginary frequency of τ_2 symmetry, indicating vibronic instability. Explicitly, the complexes PF_4^-(−1.70), AsF_4^-(−0.82), SbF_4^-(−0.65), and PCl_4^-(−0.31) are predicted to undergo C_{2v} distortions (Table 2) along one of the three S_4 axes of the parent tetrahedron, with stabilization energies δE_t (eV) in parentheses. Figure 7a illustrates for the SbF_4^- complex how the system stabilizes along the $T_d \rightarrow C_{2v}$ distortion path, with the two minima respresenting the equivalent distortions along the ±z axis (Figure 6a). By contrast, the InF_4^- polyhedron, lacking the lone pair, does not show vibrational instability. The

Table 2. Bond Distances (Å) and Bond Angles (deg) for the Geometrically Optimized C_{2v} (CN = 4) and $C_{2v}(C_{4v})$ (CN = 5) Geometries and Bond Length Changes δR (Averaged) from T_d to C_{2v} (CN = 4) and $\delta R_{ax}(D_{3h})$, $\delta R_{eq}(D_{3h})$ from D_{3h} to $C_{2v}(C_{4v})$ (CN = 5) (For Definitions See Figures 6A and 9[a]) of Some AX_4^- and AX_5^{2-} Complexes; Dissociation Enthalpies (eV) According to Eq 7a,b[b] Are Also Listed − Second and Third Line, with Solvent and Experimental[34] Values, Respectively

	δR	R_1	R_2	θ_1	θ_2	$\Delta H^{(s)}$
PF_4^-	−0.12	1.81	1.68	188	98	2.75
	−0.09	1.82	1.67	188	91	0.72
		1.74	1.60	192	100	
AsF_4^-	−0.08	1.93	1.80	186	98	2.97
SbF_4^-	−0.08	2.07	1.98	189	97	3.32
PCl_4^-	−0.04	2.41	2.15	168	100	1.23

	$\delta R_{ax}(D_{3h})$	$\delta R_{eq}(D_{3h})$	R_{ap}	$R_1 = R_2$	$\theta_1 = \theta_2$	$\Delta H^{(s)}$
PF_5^{2-}	−0.02	−0.14	1.71	1.92	86	−2.70
	−0.04	−0.15	1.72	1.89	83[c]	−0.02
AsF_5^{2-}	−0.01	−0.08	1.83	2.03	88	−2.14
SbF_5^{2-}	−0.03	−0.08	2.00	2.16	86	−1.55
PCl_5^{2-}	0.02	−0.03	2.19	2.49	95	−2.53

[a] $\delta R_{ax}(D_{3h})$: bond length change from D_{3h} (axial) to C_{4v} (equatorial, R_1). $\delta R_{eq}(D_{3h})$: bond length alteration from D_{3h} (equatorial) to C_{4v} (apical, R_{ap}). [b] Processes C_{2v}(CN = 4) → C_{3v}(CN = 3) and $C_{4v}(C_{2v})$ (CN = 5) → C_{2v}(CN = 4). [c] C_{2v} geometry, with $\theta_1 = 83°$ and $\theta_2 = 85°$ (see Figure 9).

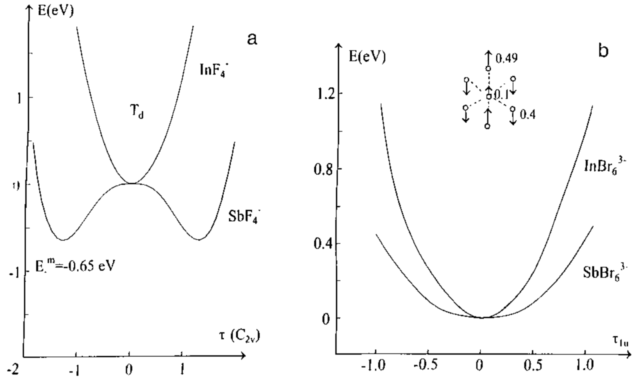

Figure 7. Potential energy plots versus the (a) τ_2-, ϵ-, and α_1-type displacements τ ($T_d \rightarrow C_{2v}$) for SbF_4^- in comparison to InF_4^- − linear scaling of the geometric changes from the T_d optimized ($R = 2.10$ Å) to the C_{2v} geometry of SbF_4^- ($R_1 = 2.07$ Å, $\theta_1 = 189°$; $R_2 = 1.98$ Å, $\theta_2 = 97°$). (b) τ_{1u} displacements for the octahedral complexes $Sb(In)Br_6^{3-}$ corresponding to the lower energy τ_{1u} mode for $SbBr_6^{3-}$ and retaining a linear variation of the given coordinates also for larger deviations from O_h; the inset represents the unit distortion ($\tau_{1u} = 1.0$).

compexes BiF_4^-, $AsCl_4^-$, $SbCl_4^-$, and PBr_4^- are found to possess either very small $|\delta E_t|$ values (<0.1 eV) or τ_2 vibrations with pronounced soft mode behavior (see Figure 7b), suggesting fluxional properties. Yet also complexes such as $AsBr_4^-$, in comparison to $GaBr_4^-$ without the lone pair, possess one rather soft τ_2 mode − $AsBr_4^-$, 169 (α_1), 212 (τ_2), 39 (ϵ), 28 (τ_2) cm^{-1}; and $GaBr_4^-$, 184 (α_1), 254 (τ_2), 55 (ϵ), 92 (τ_2) cm^{-1}. While the vibrational energies of the former complex are generally smaller by about 20%, due to the larger ionic radius of As^{3+} as compared to that of Ga^{3+}, the decrease of the lower energy τ_2 mode is much more pronounced (soft mode behavior as in Figure 7b). External strains of lower symmetry, such as small disturbances by solvent effects or cooperative elastic and/or packing effects in solids, may stabilize the system in a shallow minimum along the C_{2v} distortion path.[31]

Table 3. Energies E_-^m and E_{rf}^m, E_{vib}^m, E_{FC}^m, N^m As Calculated from the Vibronic Model (PF_3 and PF_4^- − See Appendix) and/or Estimated (See Text) from the DFT Energies in Table 1 (PF_4^-, Second Line, and PF_5^{2-}), for $PF_n^{(n-3)-}$ Polyhedra in a Solvent Continuum (in eV); the Hardness Values η_s (See Text; in eV) of the Distorted Polyhedra Are Also Listed[a]

	$E_-^{m\,b}$	E_{rf}^m	E_{vib}^m	$E_{FC}^m/2$	N^m	η_s
PF_3[c]	−2.67	2.47	5.14	4.53	4.49	7.54
PF_4^-	−1.65	2.40	4.05	3.37	3.28	5.91
	−1.65	2.7	4.4	3.37	3.2	5.91
PF_5^{2-}	−0.76	2.9	3.7	2.51	2.2	4.98

[a] For the exact definition of all quantities, see text. [b] $\delta E_t' = \delta E_t(E_-^m) + \delta E_s$ (see eq 1). [c] Bare molecule.

The origin of the less pronounced lone-pair effect, if one compares the AX_4^- complexes with the corresponding AX_3 compounds, is mainly a distinctly lower vibronic coupling energy. This is readily deduced from Table 3, where we have listed the various energy contributions according to the vibronic model (eqs 3, 4) for PF_3, PF_4^-, and PF_5^{2-} as model species. A polarized solvent continuum was added to compensate the negative charges of the latter two complexes. The energies for the PF_4^- polyhedron were calculated utilizing a procedure which is outlined in the Appendix and which follows the vibronic concept elaborated for the AX_3 molecules.[10] The calculations are based on the $E_-^m = \delta E_t' - \delta E_{solv}$ energies (eq 1) without the solvent energy contributions. Though the MO energies are strongly stabilized by the polarization effects due to the solute−solvent interaction as compared to the bare anions, E_{solv} itself has no influence on the intrinsic ground-state properties of the complex. However, the solvent does affect E_{FC}^m, because the electronic transition induces a rearrangement of the charges in the solute−solvent contact region.[32] Though this energy contribution is not precisely imaged by a solvent continuum without mass, we have included it ($E_{solv}(E_+^m) - E_{solv}(E_-^m)$) in the E_{FC}^m energies, this enhancing the total transition energies by less than 10%. The vibronic quantities collected in Table 3 are very near to those which can be estimated from the DFT energy increments in Table 1. Keeping in mind that δE_P and δE_{el} are (nearly) completely part of the restoring energy, the increase of these quantities from PF_3 via PF_4^- to PF_5^{2-} can be directly translated into a corresponding increase of E_{rf}, using the PF_3 molecule, where a complete vibronic calculation has been performed[10] as the reference (Table 3). The derived nondiagonal coupling energy N^m is found to be reduced by nearly 30% when increasing the CN from 3 to 4 and becomes smaller by about the same percentage proceeding from PF_4^- to PF_5^{2-}. A similar gradation is deduced if one analyzes the potential energy curvatures in the vicinity of the high-symmetry reference geometries (Supporting Material A). The restoring energy seems to only slightly increase if the number of ligands becomes larger, while the vibronic energy E_{vib}^m decreases, but still dominates with respect to E_{rf}^m, mostly due to N^m. Also in these cases, N^m is the energetically dominating vibronic contribution; that is, eq 5 is valid in good approximation.

We have also calculated the chemical hardness, utilizing eq 6, but with solvent addition (eq 6a). $\eta_s' = (^1/_2)(I_s' - A_s')$ is rather small, because the solvent energy stabilizes the anions

---

(31) Reinen, D.; Atanasov, M. *Magn. Reson. Rev.* **1991**, *15*, 167.

(32) Hush, N. S.; Reimers, J. R. *Chem. Rev.* **2000**, *100*, 775.

$$PF_4^- \text{ (solv)} \rightarrow PF_4^0 \text{ (solv)} + e^- \text{ (vacuo)} + I_s'$$

$$PF_4^- \text{ (solv)} + e^- \text{ (vacuo)} \rightarrow PF_4^{2-} \text{ (solv)} + A_s' \quad (6a)$$

and the more that happens, the higher the negative charge is. However, the adoption of the hardness as a measure of intrinsic complex properties is more appropriate, if used without taking the solvation energies into account (η_s).[29] The thus defined η_s values and the nondiagonal vibronic coupling energies N^m (Table 3) mirror the basic trend, that *polyhedra* $AX_n^{-(n-3)}$ *become softer with increasing coordination number n and anionic charge, and correspondingly possess a less pronounced vibronic instability*. Thus PF_4^- is located in Figure 4 near to BiF_3, while PF_5^{2-} is positioned very close to $BiCl_3$. This trend also implies that the vibronic energies E_{vib}^m of the soft complexes such as $As(Sb)Br_4^-$ and, in particular, their nondiagonal components N^m are not large enough anymore to still induce negative δE_t energies (eqs 3, 4). The quantities E_{vib}^m and N^m are still finite in magnitude though ($N^2/\delta < E_{rf}$; eq 3a), reducing the restoring energy ($E_{rf} \rightarrow E_{rf}^{eff}$) and thus inducing soft mode properties. An analysis of the various contributions from the α_1 stretching, the τ_2 stretching, and the angular τ_2 and ϵ bending modes to the vibronic coupling energy is given in the Appendix.

The optimized C_{2v} geometries are rather close to a pseudo-trigonal-bipyramid $A(X_2E)X_2$ and listed in Table 2. The angle θ_1 (see Figure 6a) is near to linearity, θ_2 is roughly 100°, and the bond lengths R_1 and R_2 differ by about ±0.06(1) Å from the average spacing in the case of the fluorides and considerably more, by ±0.13 Å, for PCl_4^-. The average distance decreases by $\delta R \approx 0.08(4)$ Å on moving from the T_d parent geometry to C_{2v}. This is readily explained by an antibonding s^2-type lone pair with repulsive properties toward the ligands (Figure 6), which adopts partly directional p_z character by vibronic mixing when passing from T_d to C_{2v}, thus avoiding stronger interactions with A−X bond electron densities. We recall that the deciding energy contribution to the stabilization of the distorted geometry is the gain in bond energy by the s−p_z hybridization.[2] The comparison with well-established structural data for the salt $(NMe_4)PF_4$ yields that the calculated spacings are too large by about 5%, while there is reasonable agreement with reported bond angles. AsF_4^- is also claimed to have a near-to-trigonal bipyramidal C_{2v} structure.[11] The salt KSb_2F_7 contains isolated SbF_3 and SbF_4^- entities, the latter with a C_{2v} distortion exceeding the one calculated (Table 2).[11] However, the DFT geometry refers to an isolated SbF_4^- complex, which is not subject to lattice strains and charge compensation; the latter influences may well shift the minimum of the rather flat potential curve (Figure 7a) to higher nuclear displacements. In the crystal structures of the anionic complexes $SbCl_4^-$, $BiBr_4^-$, and BiI_4^- with large countercations, $SbCl_4^-$ possesses a C_{2v} geometry with, in the lone-pair direction, long distance interactions to two further Cl^- ligands of neighbored complexes, while the Bi^{III} polyhedra are already close to octahedra, which possess two common ligands with adjacent polyhedra.[11] This finding is indeed consistent with a vibronic coupling strength which decreases the softer the considered entities are. The long distance interactions with two ligands from neighbored poyhedra can be either looked at as a lattice strain of C_2 symmetry, which supports the PSJT interaction, or alternatively as the consequence of a lone-pair distortion of an octahedral complex (section VII).

A clean separation of the energy changes, which occur during the $T_d \rightarrow C_{2v}$ transition along the τ_2 and, through mixing with the excited state, along the ϵ distortion path, from those induced by the α_1 stretch (bond length reduction δR, see Table 2), is generally not possible (presence of significant nondiagonal terms between the α_1 and τ_2 stretching displacements). Nevertheless, the analysis for PF_4^-, AsF_4^-, and SbF_4^-, where the angular nuclear motions induce the largest part of δE_t (Tables 1, 2), leads to essentially the same results as for the AX_3 molecules. Again, δE_P is nearly exclusively a radial α_1 effect due to the shrinking δR of the average bond length (Table 2), which does not stabilize the distorted structure. It is the orbital energy δE_{orb}, mainly the angular τ_2 and ϵ contributions (see Appendix), which enforce negative $\delta E_t = E_-^m$ energies.

If a polarizable continuum for charge compensation is included into the calculations for PF_4^-, the magnitudes of $|\delta E_P|$, $|\delta E_{el}|$, and $|\delta E_{orb}|$ become smaller by about 20%, yielding values which are only slightly larger than those of PF_3. The charge distribution has obviously changed considerably by the complex−solvent interaction, by inducing significant differences of the average bond lengths with and without solvent (Table 2); thus, δR is less strongly reduced during the $T_d \rightarrow C_{2v}$ transition than in the case of the bare species. It is remarkable, however, that δE_t changes only marginally by the solvent influence.

The MO diagram of solvated PF_4^- (Figure 6) visualizes the orbital shifts when transforming the T_d into C_{2v} geometry. Not only the a_1 MOs are involved, but also, in particular, the occupied bonding b_1 MOs, which are correlated with the phosphorus $2p_x$ orbital and the shorter R_2 spacings, participate and are strongly stabilized. This is readily deduced from Table 1, where, in contrast to the AX_3 molecules, not only $\delta E_{orb}(a_1)$, but also $(\delta E_{orb} - \delta E_{orb}(a_1))$, representing the shifts of all other MOs besides those of a_1-type, contribute strongly to the stabilization of the distorted molecule. The HOMO is antibonding with 41% 3s(P) character and stabilized via $3p_z$(P) admixture by −1.3 eV. The solvent has a stabilizing effect of about −4.4 eV on the bonding and nonbonding MOs in T_d and C_{2v}, with only rather small individual deviations of the MOs from this value. The HOMO stabilization for the bare PF_4^- anion (−0.50 eV) is much less pronounced than for the solvated complex.

We now analyze the complex stabilities with respect to the dissociation of one X^- ligand, with (ΔH^s) and without (ΔH) solvent:

$$AX_4^- \rightarrow AX_3 + X^- + \Delta H^{(s)} \quad (7a)$$

A strong solvent influence on the dissociation enthalpy is calculated for PF_4^- (Table 2). Because the small and rigid F^- anion is stabilized more strongly (−4.4 eV) than the complex (−2.5 eV) by the solvent, the polarizable continuum favors the dissociation process mainly by these energy increments (∼ −2 eV). However, PF_4^- turns out to be stable also as a solvated species ($\Delta H^s > 0$), and the trend of ΔH in the sequence from PF_4^- to SbF_4^- (bare anions) also substantiates that the complex stability increases, in accord with the experimental evidence. Figure 8a illustrates the various stabilization possibilities of the tetrahedral PF_4^- anion, with and without solvent. The complex may gain energy via three vibronically induced distortion processes, from which two, $T_d \rightarrow C_{2v}$ and $T_d \rightarrow C_{3v}$, were discussed before (see Figure 6a). The third follows the C_{3v} distortion path in the opposite direction, $T_d \rightarrow C_{3v}$(i), with

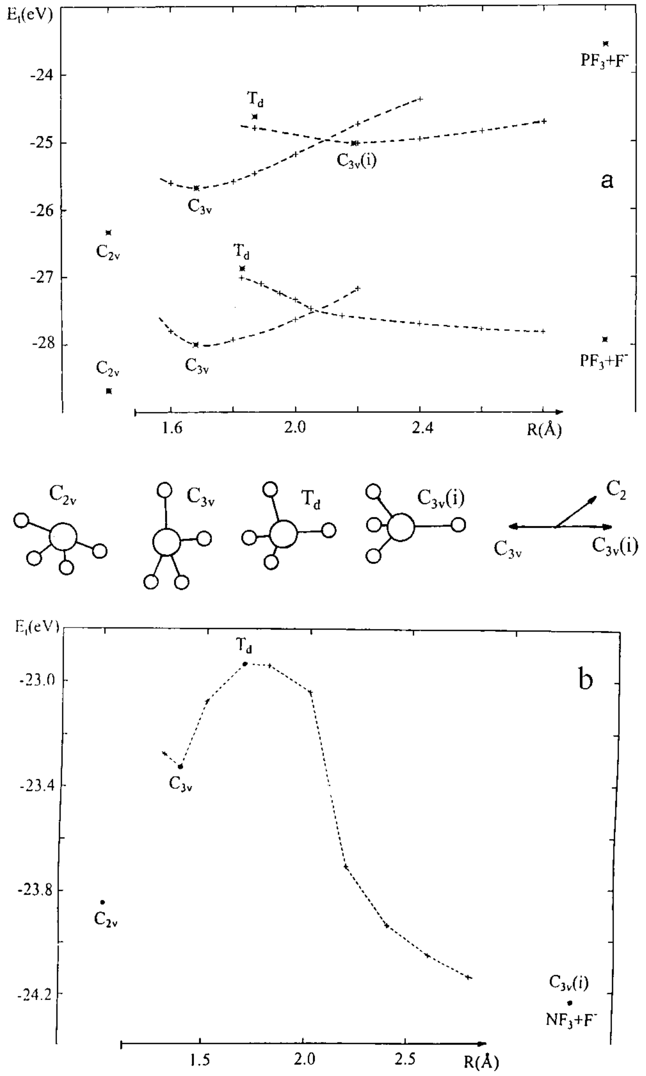

Figure 8. Total energies for the tetrahedral complexes PF_4^- (with, below, and without solvent) (a) and NF_4^- (with solvent) (b) along the C_{3v}(i) (C_{3v}) displacement path, in dependence on the long(short) P(N)−F spacing *R*. Every indicated energy was optimized with respect to the other P(N)−F spacings and the F−P(N)−F angles; the energies for the optimized C_{2v} distorted complexes are indicated on the left.

the lone pair extending toward one of the four ligands, favoring a geometry with one long and three shorter P−F spacings. While for the bare species the latter pathway leads to a relative minimum (saddle point in a multidimensional description including the dependence on all active modes) and corresponds to a finite distortion, the complete loss of one ligand according to eq 7a is predicted in the case of the solvated anion ($T_d \rightarrow C_{3v}$(i): −1.20 eV). For both the bare and the solvated PF_4^- anion, the lowest energy is calculated for the C_{2v}-type geometry of a pseudotrigonal-bipyramid $P(F_2E)F_2^-$ with $\delta E_t \cong -1.7$ eV, however (Table 1).

If one turns to the NX_4^- polyhedra (X = F, Cl) in a polarizable solvent, a distinctly different energetic situation is met, with the dissociation $T_d \rightarrow C_{3v}$(i) (−1.30 eV) preferred to the $T_d \rightarrow C_{2v}$ (−0.96 eV) and $T_d \rightarrow C_{3v}$ (−0.39 eV) distortion paths (Figure 8b). Though the driving force for the dissociation is clearly the pronounced PSJT stabilization of NF_3 ($D_{3h} \rightarrow C_{3v}$: −3.5 eV[10]), we regard the strong tendency of NX_4^- complexes to reduce the CN partly as an effect which is induced by the size mismatch between N and X, whereby the small central atom induces strong ligand−ligand repulsions in the case of larger CNs (*ionic size effect*). If one calculates the ΔH^s enthalpies of the process (7a) from T_d (AF_4^-) to D_{3h} (AF_3), considering the non-lone-pair atom A = B^{III} in comparison to N^{III}, one finds +1.07 and +2.28 eV for BF_4^-/BF_3 and NF_4^-/NF_3, respectively. These rather low energy values indicate indeed for both complexes a soft mode behavior along the C_{3v}-(i) distortion path already without taking the vibronic stabilization of NF_3 from $D_{3h} \rightarrow C_{3v}$ into account. The significance of such ionic size influence becomes apparent also in the (hypothetical, energetically less favored) C_{2v} geometries of NF_4^- (Figure 8b) and NCl_4^-; here, in contrast to the results for the other AX_4^- complexes, the stretching τ_2-type bond length changes are extremely large, the differences $R_1 - R_2$ (Figure 6a) amounting to 0.45 and 0.65 Å for X = F and Cl, respectively, a clear tendency toward a (2 + 2) coordination, that is, a reduction of the CN. Indeed, NX_4^- complexes have not been observed thus far. In contrast to the solvated NF_4^- anion, the bare complex is found to be stable toward dissociation; $\delta E_t = E_-^m$ is calculated to be −0.37 eV for $T_d \rightarrow C_{3v}$ and −0.67 eV for $T_d \rightarrow C_{2v}$ ($R_1 = 1.85$ Å, $R_2 = 1.41$ Å, $\theta_1 = 167°$, $\theta_2 = 102°$).

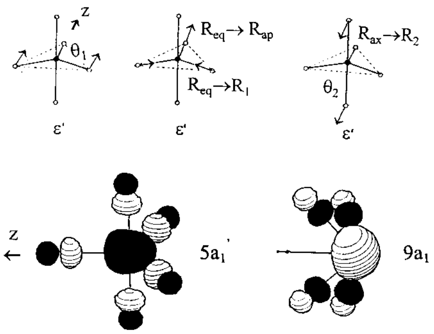

Figure 9. The highest symmetry components of the three vibronically active ϵ' modes of AX_5^{2-} complexes in D_{3d} symmetry (above), and the shapes of the HOMO in the reference (D_{3h}) and in the final (C_{2v}) optimized geometry for PF_5^{2-} (below).

It is finally interesting to note that the AX_4^- complexes in their lowest excited T_2 states are calculated by DFT to possess approximately square-planar shapes. This is in agreement with the vibronic coupling model, because this geometry (D_{4h}) is the extreme of a tetragonal D_{2d}-type compression along one of the three S_4 axes in T_d which is predicted to occur as the consequence of a first-order JT effect along the ϵ displacement path (vide supra).

VI. The Coordination Number 5

The parent symmetry of complexes AX_5^{2-} (D_{3h}) is the same as the one of the AX_3 molecules. However, in contrast to the MO scheme in Figure 3, the LUMO is not the weakly π-antibonding a_2'' MO (corresponding to the central atom p_z orbital) anymore, but a ($\sigma + \pi$)-antibonding e′ MO (originating from the central atom in-plane p_x, p_y orbitals). Because the p_z orbital of A is strongly involved in σ-interactions with the axial ligands now, it surpasses the first excited e′ MO in energy. The PSJT interaction is of $A_1' \otimes \epsilon' \otimes E'$ nature accordingly, and the vibronically active modes are the three ϵ' vibrations (one stretching, two bending) in D_{3h} (Figure 9). The corresponding displacements lead into the C_{2v} point group, eventually reaching

C_{4v} as a special geometry. The latter is close to the pseudo-octahedral coordination AX_5E predicted by the VSEPR model. The change of the s-type HOMO in D_{3h} to the corresponding MO in $C_{2v}(C_{4v})$ − here the apical ligand does not contribute − is characterized by pronounced directional p-admixture. A thorough treatment of the symmetry aspects of the $A_1' \otimes \epsilon' \otimes E'$ interaction, for five-coordinated Cu^{2+} complexes, is given elsewhere.[33]

The overall appearance of geometric distortions for AX_5^{3-} complexes is similar to the results obtained for the tetrahedral complexes. While PF_5^{2-} (−0.88), AsF_5^{2-} (−0.37), SbF_5^{2-} (−0.36), and PCl_5^{2-} (−0.14) are distinctly stabilized in a C_{4v} geometry − δE_t energies (eV) in parentheses − the other complexes show either only very small stabilization energies $D_{3h} \rightarrow C_{2v}(C_{4v})$ − δE_t between −0.06 and −0.01 eV: $PBr(I)_5^{2-}$, $AsCl_5^{2-}$, $SbCl_5^{2-}$ − or mostly soft mode behavior. Correspondingly, the first mentioned four complexes possess imaginary frequencies for one of the three ϵ' modes (actually a mixture of the three symmetrized displacements in Figure 9). The N^m/η correlation depicted in Figure 4 is also applicable to the CN = 5; a further reduction of the nondiagonal coupling term N^m and of the chemical hardness occurs, proceeding from the AX_4^- to the AX_5^{2-} complexes (Table 3). For obvious reasons − see the discussion of the NX_4^- anions in the preceding section − we do not treat NX_5^{2-} complexes.

Here the totally symmetric stretching modes (α_1' axial and equatorial) also participate in the distortion process, reducing the average bond lengths (see δR_{ax} and δR_{eq} in Table 2), with the same difficulty to exactly separate the energy contribution from the symmetry-breaking ϵ' stretching vibration from that due to the totally symmetric stretch (α_1' in-plane), if the latter adds essentially to δE_t. Nevertheless, the two examples listed in Table 1 demonstrate again that δE_P and δE_{el} represent predominantly energy effects from the two α_1' modes, while δE_t is an *orbital* effect.

The calculated polyhedron geometries (Table 2) are very near to C_{4v} with angles between the apical and the equatorial bonds of 90 ± 5°, in accordance with the approximate tetragonal pyramidal shape of SbF_5^{2-} and $SbCl_5^{2-}$ ($\delta E_t = -0.36$ and −0.02 eV, respectively). A quantitative comparison of the reported structural results with the DFT geometries makes no sense, because data for the charge-compensated complexes are not available. Turning to PF_5^{2-}, the addition of a solvent continuum does again not change δE_t essentially (Table 1), but leads to an increase of δE_P, $|\delta E_{el}|$, and $|\delta E_{orb}|$, such that they are now consistent with the trend of the corresponding energies for PF_4^- and PF_3.

The complex stabilities (eq 7b) are strongly influenced by the solvent medium (see the $\Delta H^{(s)}$ values in Table 2). The large and doubly charged PF_5^{2-} anion is stabilized in a distinctly more

$$AX_5^{2-} \rightarrow AX_4^- + X^- + \Delta H^{(s)} \tag{7b}$$

pronounced way (−9.7 eV) than both PF_4^- (−2.5 eV) and F^- (−4.4 eV), as compared to the bare complex, yielding a vanishing $\Delta H^{(s)}$ energy. Hence, a slightly negative free energy change $\Delta G^{(s)}$ is expected, because the right side of equilibrium (7b) is favored by entropy. In agreement, a PF_5^{2-} complex is not reported. Adopting a solvent stabilization energy of ~2.5 eV as a rough scaling measure, we may draw the qualitative conclusion that SbF_5^{2-}, AsF_5^{2-}, and $SbCl_5^{2-}$ ($\Delta H = -1.58$ eV) are stable species, while this is doubtful in the case of PCl_5^{2-}. The dissociation process (7b) can be looked at as mainly or partly induced by vibronic coupling. The solvated trigonal-bipyramidal PF_5^{2-} complex, for example, may gain energy either by distortion along one C_2 axis toward the PF_5E^{2-} geometry − PF_5^{2-} (D_{3h}) → PF_5^{2-} ($C_{2v} \approx C_{4v}$) − or by a distortion in the inverse direction C_{2v}(i) − PF_5^{2-} (D_{3h}) → PF_4^- (C_{2v}) + F^- − with the lone pair sticking out toward one of the in-plane F^- ligands (see Figure 9). Both alternatives lead to the same stabilization energy of about −0.8 eV (Tables 1, 2), the entropy contribution rather favoring the C_{2v} distorted PF_4^- polyhedron than the PF_5^{2-} anion with C_{4v} geometry, as just discussed. This consideration is analogous to that in section V, where also two vibronic pathways in opposite directions were proposed.

Table 4. Dissociation Enthalpies According to Eq 8, without (ΔH) and with (ΔH^s)[a] a Polarizable Solvent Continuum (in eV), for PF_6^{3-} and SbF_6^{3-} in Comparison to the Non-Lone-Pair Complexes AlF_6^{3-} and InF_6^{3-}

	ΔH_5	ΔH_4	ΔH_3	ΔH_5^s	ΔH_4^s	ΔH_3^s
PF_6^{3-} [b]	−7.23	−9.93	−7.18	−0.68	−0.70	−0.03
PF_6^{3-} [c]	−6.35	−8.23	−4.50	0.38	0.78	2.70
AlF_6^{3-} [c]	−6.67	−8.94	−3.78	0.51	1.09	4.00
SbF_6^{3-} [b]	−5.76	−7.31	−7.01	0.0	0.7	1.9
SbF_6^{3-} [c]	−5.40	−6.66	−5.35	0.4	1.4	3.6
InF_6^{3-} [c]	−5.66	−3.99	−2.44			

[a] Estimated enthalpies for SbF_6^{3-} (see section II). [b] For the processes eq 8 from AF_6^{3-} (O_h) to AF_5^{2-} (C_{4v}), AF_4^- (C_{2v}), and AF_3 (C_{3v}), respectively; A = P, Sb. [c] For the processes eq 8 from AF_6^{3-} (O_h) to AF_5^{2-} (D_{3h}), AF_4^- (T_d), and AF_3 (D_{3h}), respectively; A = P, Sb.

VII. The Coordination Number 6

Geometrical instability of an octahedral AX_6^{3-} complex may occur, if the $A_{1g}(ns^2)$ ground state interacts with the T_{1u} excited state, corresponding to the transfer of a single electron from the antibonding a_{1g} HOMO into the more strongly antibonding t_{1u} LUMO in the simplest case (Figure 1, section III). The involved vibrations are the bending and stretching τ_{1u} symmetrized displacements which mix with the α_{1g} and ϵ_g modes in the case of C_{4v}, or with α_{1g} and τ_{2g} if C_{3v} and C_{2v} distortions are considered. All geometrically optimized octahedral complexes AX_6^{3-} (A = P, As, Sb, Bi; X = F, Cl, Br, I), with the exception of PF_6^{3-}, AsF_6^{3-}, and SbF_6^{3-}, possess real vibrational energies, implying an energy minimum at octahedral geometry. The same result holds for the solvated anions, though the vibrational energies get larger (see section II). In contrast, the dissociation enthalpies ΔH for the bare complexes (eq 8, Table 4) are strongly negative in all cases. We must, therefore, regard the *bare* AX_6^{3-} anions with O_h energy minima as metastable.

$$\begin{aligned} AF_6^{3-} &\rightarrow AF_5^{2-} + F^- + \Delta H_5^{(s)} \\ AF_6^{3-} &\rightarrow AF_4^- + 2F^- + \Delta H_4^{(s)} \\ AF_6^{3-} &\rightarrow AF_3 + 3F^- + \Delta H_3^{(s)} \end{aligned} \tag{8}$$

The finding of minima at regular O_h geometries for almost all AX_6^{3-} octahedra confirms the key observation that with increasing CN the vibronic activity of the lone pair decreases, though it does not vanish. Indeed, if one compares, for example, Sb^{III} with the corresponding closed shell system without the

---

(33) Reinen, D.; Atanasov, M. *Chem. Phys.* **1989**, *136*, 27; **1991**, *155*, 157.

lone pair (In^{III}), the rather flat potential surface of $SbBr_6^{3-}$, for example (Figure 7b), suggests soft mode behavior ($E_{vib} < E_{rf}$); already small external disturbances may modify it such that energy minima appear at finite τ_{1u} nuclear displacements. In accord with such a concept, Sb^{III} appears in a regular octahedron in the mixed-valent compound $(NH_4)_4[(Sb^{III}Br_6)(Sb^{V}Br_6)]$,[35] while the strain along the C_3 axis in the complex anions $A_2Br_9^{3-}$ ($A = Sb^{III}$, Bi^{III}), two octahedra with a common face, induces a considerable C_{3v} distortion with short(long) A−Br distances of 2.63(3.00) Å for Sb^{III} and 2.94(3.24) Å for Bi^{III}.[11] In the hexagonally close-packed structures of AsI_3, SbI_3, and BiI_3 − where again a lattice strain along C_3 is present − one observes highly C_{3v} distorted AsI_6^{3-} [11] and regular BiI_6^{3-} octahedra,[36] with SbI_6^{3-} representing an intermediate case.[11] A strain of C_2 symmetry is encountered in $(H_2DAH)BiI_5$ (DAH = diaminocyclohexane),[37] where one BiI_6^{3-} octahedron shares cis-vertexes with two neighbored octahedra in one-dimensional zigzag chains. Here, three pairs of Bi−I bonds appear: *bridging* ones (3.30 Å), terminal ones trans to the bridging I^- ligands (2.91, 2.96 Å), and terminal ones perpendicular to the chain (3.06, 3.10 Å), yielding in good approximation C_{2v} distorted octahedra. Analogous compounds with even larger countercations have been recently reported.[38] All of these examples nicely follow the trend of the hardness rule according to Figure 4.

Turning to the vibronically unstable species PF_6^{3-}, AsF_6^{3-}, and SbF_6^{3-}, we first note that in particular PF_6^{3-} possesses enthalpies ΔH and ΔH^s according to eq 8, which are rather similar to those of the non-lone-pair complex AlF_6^{3-}, *if the additional vibronic stabilization energies from* D_{3h} *to* C_{4v}, T_d *to* C_{2v}, *and* D_{3h} *to* C_{3v} *for* PF_5^{2-}, PF_4^-, *and* PF_3, *respectively, are excluded* (Table 4). The solvated AlF_6^{3-} anion is calculated to be stable with respect to dissociation, as would be the PF_6^{3-} complex without taking the lone-pair stabilization energies of the five-, four-, and three-coordinate entities into account. Otherwise one finds that PF_6^{3-} should undergo dissociation, yielding the butterfly-shaped PF_4^- as the stable entity ($\Delta G_4^s < \Delta G_5^s$). Figure 10 illustrates the C_{4v}, C_{2v}, and C_{3v} displacement pathways of the solvated PF_6^{3-} anion in dependence on R, the latter denoting the long bond lengths of the distorted complex (one, two, and three, respectively); every point corresponds to a geometry optimization in which only the respective R spacing is kept constant. It is interesting that the ΔH_3^s curve displays a (relative) minimum at a finite distortion on the C_3 displacement path, which is more stable than the completely ($PF_3 + 3F^-$) dissociated complex. One vibration calculated for this geometry possesses an imaginary frequency, specifying the relative minimum as a saddle point in the multidimensional $\Delta H^{(s)}$ versus τ_{1u} space − as expected, because the final geometry with the lowest energy is C_{2v} (ΔH_4^s).

We conclude from the ΔH^s enthalpies that it is the vibronic interaction which causes the geometric instability. However, the dissociation energy is already small without the vibronic effect (AlF_6^{3-} and PF_6^{3-} in Table 4^c), indicating a rather flat potential surface. This effect enhances the extent of the vibronic geometry change and eventually leads to the complete loss of one (C_{4v}, CN = 5) or two (C_{2v}, CN = 4) ligands. Phenomena of this kind are particularly pronounced, if the central ion-to-ligand size ratio becomes smaller than a certain critical value. We prefer to separate this *ionic size effect* from the lone-pair phenomenon (section III), though one may regard it as induced by vibronic coupling as well.[39]

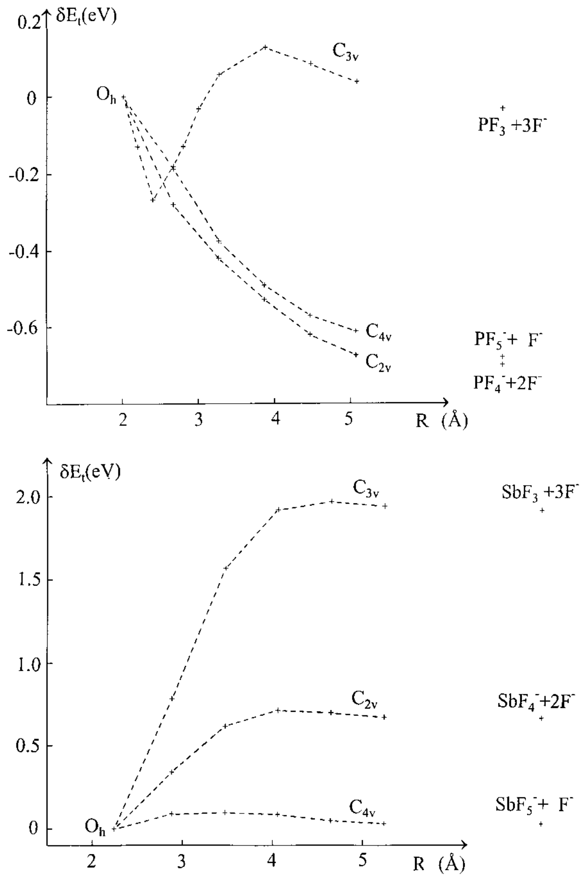

Figure 10. The dissociation displacement paths according to the processes (eq 8) for the solvated complexes PF_6^{3-} (above) and SbF_6^{3-} (below). The minimum energies for the optimized geometries are plotted versus the longer spacings of the C_{4v}, C_{2v}, and C_{3v} distorted octahedra; the enthalpies for the complete dissociation ($R \to \infty$) are given on the right.

Recalling that solvation tends to strongly stabilize highly charged anionic complexes toward dissociation (see Table 4), the solvated SbF_6^{3-} complex is expected to be stable only in the absence of vibronic coupling, similar to PF_6^{3-}. Otherwise, distinctly positive ΔH_4^s and ΔH_3^s values, but a vanishing ΔH_5^s and hence a negative ΔG_5^s energy, result. In agreement with this analysis, SbX_6^- entities with $X = Cl^-, Br^-, I^-$ are well characterized,[11] while the fluoride complex has not been synthesized so far. Figure 10 illustrates the energetic situation for SbF_6^{3-}.

We summarize that the tendency toward smaller vibronic coupling effects when increasing the CN from 5 to 6 is further continued, with only three vibronically unstable six-coordinate complexes AF_6^{3-} ($A = P^{III}$, As^{III}, Sb^{III} − solvated) left. A discussion of the bond covalency based on the MO schemes and the vibronic coupling model is given in the Supporting Information for PF_6^{3-} and BiF_6^{3-} as model examples.

---

(34) Wiberg, N. *Lehrbuch der Anorganischen Chemie*; Walter de Gruyter: Berlin, New York, 1995; p 755.
(35) Lawton, S. L.; Jacobson, R. A. *Inorg. Chem.* **1966**, *5*, 743.
(36) Ruck, M. *Z. Kristallogr.* **1995**, *210*, 650.
(37) Mousdis, G. A.; Papavassiliou; Terzis, A.; Raptopoulou, C. P. *Z. Naturforsch.* **1998**, *53b*, 927.
(38) Mitzi, D. B.; Brock, P. *Inorg. Chem.* **2001**, *40*, 2096.
(39) Bersuker, I. B.; Stavrov, S. S. *Coord. Chem. Rev.* **1988**, *88*, 1.

VIII. Summary and Conclusions

It was the purpose of this contribution to analyze the stereochemical and energetic activity of lone pairs in terms of certain chemical parameters. Molecules and complexes $AX_n^{-(n-3)}$ ($A = N$ to Bi; $X = F$ to I; $n = 3-6$) were chosen as model examples:

(1) The vibronic coupling model is a pictorial and sensible approach, which does not only provide precise information about the nuclear displacements from the high-symmetry parent geometry to that of the distorted one, but also yields criteria, whether a distortion occurs or not. Utilizing calculated DFT energies, the key parameters, which govern the geometry change, can be derived, such as the vibronic energy $E_{vib}{}^{m}$ and its nondiagonal component N^{m}. The tetrahedral complexes (vibronically active modes: τ_2, ϵ) are found to eventually distort along a C_2 axis ($\rightarrow C_{2v}$), the C_3 path ($\rightarrow C_{3v}$) being less favored. The trigonal-bipyramidal complexes are predicted to deform toward C_{4v} (active modes, ϵ'), while some octahedral complexes (active modes, τ_{1u}, ϵ_g) undergo dissociation as the consequence of vibronic coupling.

(2) The quantity, which dominates lone-pair distortions in the considered cases, is the vibronic coupling stength. It is correlated with an observable quantity, the chemical hardness (Figure 4), implying that the harder a lone-pair compound AX_3 and its constituents are, the more susceptible to distortion the molecule becomes. Proceeding to the (charge-compensated) complexes (CN $= 4-6$), one additionally finds that the higher the CN and the negative charge of a lone-pair complex are, the softer and the more stable the complex becomes toward deformation. Thus, while all AX_3 molecules distort, only part of the AX_4^- and AX_5^{2-} complexes deform. Nearly all octahedral AX_6^{3-} complexes remain in the O_h geometry with a stereochemically s^2 inert pair, with the exception of those with $A =$ P, As, Sb, and $X =$ F.

(3) The extent of distortion away from the parent geometry depends not only on the vibronic coupling but also on the restoring energy, which is frequently very small due to *ionic size* effects (section VII). Such soft mode behavior can lead to complete dissociation in the case of vibronic instability (i.e., $SbF_6^{3-} \rightarrow SbF_5^{2-} + F^-$) or $-$ if the complex is vibronically stable in the high-symmetry parent symmetry $-$ frequently to pronounced sensitivity toward external strains (imposed by the host structure, for example).

(4) The vibronic coupling effect turns out to be a pure orbital overlap phenomenon due to s$-$p mixing creating a new covalency.[5] It inevitably accompanies geometric distortions according to the vibronically active symmetry-breaking modes. The observed increase of the electron pair repulsion is mainly caused by the decrease of the average bond length, which usually accompanies the s^2-lone-pair distortion. Hence, the VSEPR energy of exchange (Pauli) repulsion δE_P (and similarly δE_{el}) does not contribute significantly to the energy balance of the lone-pair effect, if only the symmetry-breaking angular distortions are considered.

(5) The possibility to place the anionic complexes into a polarizable solvent continuum for charge compensation has contributed much to make the DFT results more realistic. The energy correction with respect to the bare anions is considerable for the highly charged complexes.

It is tempting to relate these results to the VSEPR model,[9] which considers the Pauli repulsion between the valence shell electron pairs and/or, in its recent modification, the energies connected with the *ligand close packing* concept as the driving force for the lone pair distortion. We think that both aspects refer to the restoring energy in the vibronic theory rather than to the vibronic stabilization, which is a *bonding phenomenon* (see under (4)) not considered in the mentioned approaches. The statement of L. S. Bartell in ref 14 that "there does seem to be a VESPR component over and above that of pure ligand packing" (the vibronic coupling energy) is well in line with this argument.

The applied vibronic coupling model, based on calculated DFT energies, and the derived *hardness rule* (see under (2)) have the potential to semiquantitatively analyze and systematize the stereochemical and energetic consequences of the lone-pair effect. Hopefully, the present concept at last weakens the textbook statement[11] concerning a theoretical deficiency, mentioned in the Introduction. In a further study, the authors intend to extend the investigation to the halides of the sixth and seventh main group and corresponding complexes, to check whether the derived principles are more broadly applicable.

Acknowledgment. The authors gratefully acknowledge financial support by the "Deutsche Forschungsgemeinschaft". They further thank Prof. Dr. W. J. A. Maaskant (Leiden, The Netherlands) for helpful discussions of the basic model and Prof. Dr. L. S. Bartell (Ann Arbor, MI) for valuable suggestions.

Appendix

An exact solution of matrix (eq 2), but including the coupling to the α_{1g} mode and to the symmetry-breaking ϵ_g and τ_{2g} vibrations, has been presented and discussed by Maaskant and Bersuker,[40] with a few simplifications and within the two-state model. We follow here a different philosophy, because the DFT analysis provides numerical results, which allow one to determine a larger number of unknown quantities. In analogy to the procedure applied to AX_3 molecules,[10] where the two-state model is a good approximation in most cases, we sketch here the calculation of the parameters N^m, $E_g{}^m$, $E_e{}^m$, and $E_{rf}{}^m$ (eqs 3, 4) for the CN $= 4$. It is based on the parametrization of the appropriate vibronic matrix, which is formally equivalent to the one for the octahedral case (section III).

1. CN = 4. Restricting to distortions toward C_{2v}, the 4×4 can be reduced to a 2×2 matrix, including the ground state and one split component of the excited $T_2(T_d)$ state (eq A1).

$$\begin{array}{cc} A_1(s^2) & T_2(s^1p_z{}^1) \\ E_g & N \\ N & E_e \end{array} \qquad \text{(A1)}$$

$$E_g = (^1/_2)K_b\tau_b{}^2 + (^1/_2)K_\epsilon\tau_\epsilon{}^2 - K_3\tau_\epsilon{}^3 + (^1/_2)K_s\tau_s{}^2 + (^1/_2)K_\alpha\tau_\alpha{}^2$$

---

(40) Maaskant, W. J. A.; Bersuker, I. B. *J. Phys.*: *Condens. Matter* **1991**, *3*, *37*.

$$E_{\mathrm{e}} = \delta + (^1/_2)K_{\mathrm{b}}'\tau_{\mathrm{b}}^{\;2} + (^1/_2)K_{\epsilon}'\tau_{\epsilon}^{\;2} + t_{\epsilon}\tau_{\epsilon} + (^1/_2)K_{\mathrm{s}}'\tau_{\mathrm{s}}^{\;2} + (^1/_2)K_{\alpha}'\tau_{\alpha}^{\;2} + t_{\alpha}'\tau_{\alpha}$$

$$N = t_{\mathrm{b}}\tau_{\mathrm{b}} + t_{\mathrm{b}\epsilon}\tau_{\mathrm{b}}\tau_{\epsilon}^{\;2} + t_{\mathrm{s}}\tau_{\mathrm{s}} + t_{\alpha\mathrm{s}}\tau_{\mathrm{s}}\tau_{\alpha}$$

τ_{b}, τ_{ϵ}, τ_{s}, and τ_{α} denote the bending $\tau_2(\zeta)$, $\epsilon(\theta)$ and stretching $\tau_2(\zeta)$, α_1 symmetrized displacements in T_d (Figure 6a; eq A2). $\delta\theta_1$ and $\delta\theta_2$ are the polar angles defined with respect to the S_4 axis, and $\delta\theta_{\pm}$ and $\delta\theta_{\mathrm{av}}$ are their out-of-phase and in-phase

$$\tau_{\mathrm{b}} = (1/\sqrt{2})R(\delta\theta_1 - \delta\theta_2) = \sqrt{2}R\delta\theta_{\pm}$$

$$\tau_{\epsilon} = (1/\sqrt{2})R(\delta\theta_1 + \delta\theta_2) = \sqrt{2}R\delta\theta_{\mathrm{av}}$$

$$\tau_{\mathrm{s}} = (^1/_2)(\delta R_1 + \delta \mathrm{R}_1' - \delta R_2 - \delta R_2') = 2\delta R_{\pm} \tag{A2}$$

$$\tau_{\alpha} = (^1/_2)(\delta R_1 + \delta R_1' + \delta R_2 + \delta R_2') = 2\delta R_{\mathrm{av}}$$

changes ($\delta\theta_{\mathrm{av}} > 0$ for D_{2d} compression). $\delta R_1 = \delta R_1' = |\delta R_2| = |\delta R_2'|$ denote A−X bond length alterations and $\delta R_{\pm}$, δR_{av} the corresponding out-of-phase and in-phase changes, pertinent to τ_{s} and τ_{α}, respectively. $t_{\alpha}' = K_{\alpha}'\tau_{\alpha}^{\circ}$ is a contribution due to the displacement τ_{α}° of the T_2 potential curve with respect to that of the ground state, and $K_{\mathrm{b}}(K_{\mathrm{b}}')$, $K_{\mathrm{s}}(K_{\mathrm{s}}')$, $K_{\alpha}(K_{\alpha}')$, and $K_{\epsilon}(K_{\epsilon}')$ are the force constants for the ground (excited) state. The coupling constants t_{ϵ} and t_{α} account for the shift of the energy minimum of the excited-state potential surface with respect to the ground state along the τ_{ϵ} and τ_{α} coordinates, while t_{b} and t_{s} induce the PJT-mixing. The nonlinear vibronic constants $t_{\mathrm{b}\epsilon}$ and $t_{\alpha\mathrm{s}}$ allow for the coupling between the two bending and between the two stretching modes, respectively, because any $\tau_{\mathrm{b}}(\tau_{\mathrm{s}})$ displacement is always accompanied by certain $\tau_{\epsilon}(\tau_{\alpha})$-type geometry changes. The various unknown parameters in eq A1 have been determined as follows:

K_{ϵ} , K_{ϵ}', and the higher-order force constant K_3 for the ϵ-mode, as well as the excited-state JT-coupling constant t_{ϵ}, have been deduced from DFT calculations, in which the energy changes of the A_1 and T_2 states solely due to the τ_{ϵ} distortions were considered; K_{α}, K_{α}' and t_{α}' were obtained by only varying the P−F bond lengths. All mentioned parameters have been adopted without change in eq A1. The remaining unknowns were determined in two successive steps. First, an angular DFT geometry optimization in C_{2v} symmetry (only τ_{b} and τ_{ϵ} displacements) was performed, with the bond distances fixed at the T_d values, yielding K_{b}, K_{b}', t_{b}, $t_{\mathrm{b}\epsilon}$ from the angular (a) values of $(E_-{}^{\mathrm{m}})_{\mathrm{a}}$, $(E_{\mathrm{FC}}{}^{\mathrm{m}})_{\mathrm{a}}$, $(\tau_{\mathrm{b}}{}^{\mathrm{m}})_{\mathrm{a}}$, and $(\tau_{\epsilon}{}^{\mathrm{m}})_{\mathrm{a}}$. The second step was a complete geometry optimization, from which, after adopting K_{b}, K_{b}', t_{b}, $t_{\mathrm{b}\epsilon}$ from the first step, the remaining parameters K_{s}, K_{s}', t_{s}, t_{α} were deduced. The obtained geometrical data and DFT energy changes ($T_d \rightarrow C_{2v}$) for the bare PF_4^- complex are listed in Table A3. The angular parameters from the ($\tau_{\mathrm{b}} + \tau_{\epsilon}$) optimization (step 1) are very close to those from the full optimization (step 2), this justifying the neglect of terms, which mix angular and radial displacements. The most significant vibronic energy increments (full optimization and angular changes only, first and second line, respectively) for PF_4^- are collected in Table A4.

step	$R_2(R_1)$	$\theta_2(\theta_1)$	$E_-{}^{\mathrm{m}}$	$E_{\mathrm{FC}}{}^{\mathrm{m}}$	$\tau_{\mathrm{b}}{}^{\mathrm{m}}$	$\tau_{\epsilon}{}^{\mathrm{m}}$	$\tau_{\mathrm{s}}{}^{\mathrm{m}}$	$\tau_{\alpha}{}^{\mathrm{m}}$
T_d	1.87(1.87)	55°(125°)	0	3.96	0	0	0	0
$C_{2v}(1)$	1.87(1.87)	99°(188°)	−1.10	5.71	2.03	1.56	0	0
$C_{2v}(2)$	1.68(1.81)	98°(188°)	−1.70	6.39	2.06	1.54	0.09	−0.25

(A3)

	N^{m}	$\delta E_{\mathrm{g,e}}{}^{\mathrm{m}}$	$E_{\mathrm{FC}}{}^{\mathrm{m}}$	$E_{\mathrm{vib}}{}^{\mathrm{m}}$	$E_{\mathrm{rf}}{}^{\mathrm{m}}$	$E_-{}^{\mathrm{m}}$
PF_4^-, bare	2.99	−2.27	6.39	4.33	2.63	−1.70
	2.84	0.44	5.71	2.64	1.53	−1.10
PF_4^-, solv	3.57	−0.91	7.20	4.05	2.40	−1.65
	3.30	0.99	6.67	2.84	1.66	−1.18

(A.4)

We could not use normal coordinates because the deviations of the distorted from the parent structures are usually very large. Instead, we employ the symmetrized displacements pertinent to the DFT optimized geometries in the minima of the potential energy curves. The derived force constants, which are effective because higher-order terms are neglected, bear no physical significance and are only needed to reliably estimate the crucial restoring energy $E_{\mathrm{g}}{}^{\mathrm{m}} \equiv E_{\mathrm{rf}}{}^{\mathrm{m}}$ (eq A1). Utilizing the DFT energies $E_-{}^{\mathrm{m}}$ and $E_{\mathrm{FC}}{}^{\mathrm{m}}$ (eqs 3, 4), $E_{\mathrm{vib}}{}^{\mathrm{m}}$ and N^{m} can then be determined.

As for the AX_3 molecules, the nondiagonal vibronic coupling (N^{m}) is of predominantly angular origin. The radial changes enhance the vibronic interaction energy $E_{\mathrm{vib}}{}^{\mathrm{m}}$ by affecting strongly the diagonal coupling contributions $\delta E_{\mathrm{g,e}}{}^{\mathrm{m}}$. This enhancement is largely compensated by an increase of the restoring energy, leading to an only moderate contribution to the total stabilization energy. The solvent addition leaves $E_{\mathrm{vib}}{}^{\mathrm{m}}$, $E_{\mathrm{rf}}{}^{\mathrm{m}}$, and hence $E_-{}^{\mathrm{m}}$ nearly unchanged, though N^{m} increases significantly. Though the two-state approximation is not strictly valid in the PF_4^- case − there are two further excited T_2 states at 7.4 and 8.1 eV present besides the one at 4.8 eV (bare anion) − the respective influence on the vibronic coupling energy is only small, as was explicitly checked.

2. CN = 3. Because there is only one symmetry-breaking mode α_2'', the coupling matrix is of the form A1; the nondiagonal term N ($= t_{\alpha}\tau_{\alpha} + t_{\alpha\mathrm{r}}\tau_{\mathrm{r}}\tau_{\alpha}$) contains the vibronic interaction constants t_{α} and $t_{\alpha\mathrm{r}}$, where t_{α} refers to α_2'', and $t_{\alpha\mathrm{r}}$ mirrors the mixing of the bending α_2'' with the totally symmetric α_1 displacement. A combined DFT-vibronic coupling calculation has been performed for this class of compounds within the two-state model, critically commenting on the validity of this approximation.[10] We only note here, in addition, that the definition of the restoring energy $E_{\mathrm{rf}}{}^{\mathrm{m}}$ given here (eq 4) differs from the approximate one in eq 8a of ref 10. There, the initial splitting δ had been introduced instead of $\delta E_{\mathrm{g,e}}{}^{\mathrm{m}}$, because δ is more easily accessible.

Supporting Information Available: Vibronic coupling studies (PDF). This material is available free of charge via the Internet at http://pubs.acs.org.

JA012408H